Ar$^+$ and Xe$^+$ Velocities near the Presheath-Sheath Boundary in an Ar/Xe Discharge

J. T. Gudmundsson[1,2,3] and M. A. Lieberman[1]

[1]*Department of Electrical Engineering and Computer Sciences, University of California, Berkeley, California 94720, USA*
[2]*University of Michigan-Shanghai Jiao Tong University Joint Institute, Shanghai Jiao Tong University, Shanghai 200240, China*
[3]*Science Institute, University of Iceland, Dunhaga 3, IS-107 Reykjavik, Iceland*

The velocities of Ar$^+$ and Xe$^+$ ions near the presheath-sheath boundary in an Ar/Xe discharge are studied by particle-in-cell Monte Carlo simulation. For a pure argon discharge the argon ion has almost the same velocity profile as it does in the mixture of argon and xenon. Similarly, for a xenon discharge the xenon ion has almost the same velocity profile as it does in the mixture of argon and xenon. The ion speed at the sheath-presheath boundary is the same for an ion in a pure argon or xenon discharge and for the same ion in a mixture of argon and xenon. We conclude that, in our simulation, each ion reaches its own Bohm speed at the presheath-sheath interface.

The question of how the velocities of ions are determined at the presheath-sheath boundary in plasmas with multiple-ion species is of fundamental interest in various fields of plasma physics and has gained interest lately [1–8]. In a weakly collisional plasma with a single-ion species, where the ion collisional mean free path is significantly larger than the Debye length, a presheath develops in the plasma and ions are accelerated to the Bohm speed (ion sound speed) at the presheath-sheath edge

$$u_B = \left(\frac{eT_e}{M}\right)^{1/2}, \tag{1}$$

where T_e is the electron temperature and M is the ion mass [9]. This condition is commonly referred to as the Bohm criterion. For multiple-ion species a generalized Bohm criterion has been derived [10]

$$\sum_j \left(\frac{n_j}{n_e}\right)\frac{u_{Bj}^2}{u_j^2} \leq 1, \tag{2}$$

where the sum is over the number of ion species, u_j is the ion drift velocity at the presheath-sheath edge, n_j is the ion density, n_e is the electron density, and the equality is usually assumed. However, this criterion leads to an infinite number of possible solutions. Two simple solutions are apparent. First, all ions reach the sheath edge with the same velocity, the ion sound speed of the system. Second, each ion species has its own Bohm speed at the sheath edge. Lee *et al.* [5] argue using dispersion relations along with the generalized Bohm criterion (2) for two positive ion species plasma that each ion species has the bulk ion sound velocity at the presheath-sheath boundary. Baalrud *et al.* [6,7] claim that for roughly equal densities of cold ions a collisional friction associated with ion-ion two stream instability will bring the two ion species drift velocities closer together, and each ion species leaves the plasma at the common sound speed, while for finite ion temperature, the

ions can enter the sheath near the common sound speed, or near the individual sound speeds u_{Bj}, depending on the temperature. Franklin [3,4] argues that for an active plasma that contains more than one species of positive ions generated by electron impact ionization, each ion reaches its own Bohm speed at the presheath-sheath interface.

Lee *et al.* [1,2] applied laser-induced fluorescence (LIF) in an Ar/Xe plasma to measure the argon and xenon ion velocity distribution near a negatively biased plate. They concluded that the Ar$^+$- and Xe$^+$-ion velocities near the presheath-sheath boundary approach the common ion sound speed in the discharge. Similar findings have been reported for Ar/He plasma where the ions Ar$^+$ and He$^+$ approach a speed equal to the ion sound speed of the system [11]. The experimental results of Lee *et al.* [1,2] are the motivation for our work. Particle-in-cell Monte Carlo collision (PIC-MCC) simulations are a well-established tool to explore plasma kinetics [12]. We use the one-dimensional object-oriented plasma device code OOPD1 [13], which is partially an reduction of the XOOPIC code [14], and apply it to explore the argon and xenon ion velocities near the presheath-sheath boundary. The basic idea is to use hundreds of thousands of computer-simulation particles (superparticles) to represent a significantly higher number (10^{12}–10^{16} m^{-3}) of real particles in a laboratory device. The interaction between charged and neutral particles is treated by a Monte Carlo collision scheme that incorporates the null collision method [15] originally implemented in the XPDP1 PIC-MCC code.

The reaction set and cross sections we use have been revised significantly from the earlier work of Vahedi and Surendra [15]. The cross section for e-Ar elastic scattering is taken from Ferch *et al.* [16] and de Heer *et al.* [17]. The cross section for electron impact excitation to the $4s$ states of argon is taken from the collection of Hayashi [18] and the cross sections for the metastable $^3P_2$ and $^3P_0$ levels are

combined to give one level and the cross sections for the radiative $^1P_1$ and $^3P_1$ levels are combined to give one level. The cross section for electron impact excitation to the $4p$ manifold, assigned a threshold of 13.2 eV, the higher-energy manifolds (groups II and III assigned thresholds of 14.09 and 14.71 eV, respectively) are taken from Eggarter [19] and to the highest lying states are taken from the Hayashi collection [18] with a threshold 15.20 eV. The cross section for electron impact ionization of argon is based on the work of Krishnakumar and Srivastava [20] and Vikor et al. [21]. The cross section for elastic scattering Ar^+-Ar is taken from Cramer [22] for the energy range 4–400 eV and extrapolated to higher and lower energies. The cross section for Ar-Ar elastic scattering is taken from the theoretical work of Phelps et al. [23]. The cross section for Ar^+-Ar resonant charge exchange is taken from Hegerberg et al. [24] and Cramer [22], and is extrapolated to higher and lower energies. The cross section for e-Xe elastic scattering is from Mozumder [25]. The cross sections for excitation to the metastable levels $^3P_0^0$ and $^3P_2^0$ at 9.447 and 8.315 eV, respectively [26], the radiative level $^3P_1^0$ at 8.437 eV [26], and to the higher levels which we assign a threshold of 9.570 eV (the $^1P_1^0$ state) are taken from Sakai et al. [27]. The cross section for electron impact ionization of Xe is taken from the measurements by Rapp and Englander-Golden [28]. The cross section for Xe-Xe elastic scattering is taken from the theoretical work of Phelps [29] and for the Xe^+-Xe resonant charge exchange is from Piscitelli et al. [30]. The cross section for Xe-Ar scattering is assumed to be the average of the cross sections for Xe-Xe and Ar-Ar elastic scattering. The cross section for Xe^+-Ar elastic scattering is assumed to be the same as for Ar^+-Ar elastic scattering, and the cross section for Ar^+-Xe elastic scattering is assumed to be the same as for Xe^+-Xe elastic scattering. Long-range Coulomb interactions between charged particles, over length scales greater than or of order a Debye length, are included in the simulation, but short-range ion-ion Coulomb collisions are neglected.

The simulation attempts to model the multidipole experimental configuration described by Lee et al. [1,2]. The simulation discharge is maintained between two equal-area electrodes (1.77×10^{-2} m²) separated by a gap of 10 cm. The left hand electrode is biased at -30 V to generate an ion sheath. Three cases were simulated, a pure argon discharge at 0.7 m Torr, a pure xenon discharge at 0.7 m Torr and an argon-xenon discharge with argon and xenon partial pressures 0.5 and 0.2 m Torr, respectively. To model the ionization created by the energetic electrons in the multidipole chamber, we use a volume source with a uniform ionization rate of 4.3×10^{-19} m^{-3} s^{-1} to maintain the steady state; electrons are created with electron temperature of 0.88 eV, and ions with temperature of 32 meV. The simulation grid is uniform and consists of 2000 cells. The electron time step is chosen to be 3.6×10^{-11} s. Both the grid spacing and the time step

are chosen to resolve accurately the electron Debye length of the low energy electrons and the plasma frequency, respectively. Approximately 350 000 superparticle electrons and positive ions were used in the simulations. The simulations were run to a steady state (approximately 130 microseconds), and the diagnostics were gathered averaging over 500 000 time steps.

The plasma potential variation with distance from the biased plate is shown in Fig. 1, and the corresponding density profiles of the charged particles versus distance for a discharge with argon and xenon partial pressures 0.5 and 0.2 m Torr, respectively, are shown in Fig. 2. For a pure argon discharge at 0.7 m Torr the measured electron density is 3.48×10^{15} m^{-3} and the effective electron temperature 0.88 eV [1]. The simulations give a bulk electron temperature of 0.34 eV and an electron density of 4.7×10^{15} m^{-3}. For the Ar/Xe mixture the simulations give a bulk electron temperature of 0.34 eV and an electron density of 5.6×10^{15} m^{-3} compared to a measured electron temperature of 0.69 eV and an electron density of 8.4×10^{15} m^{-3} [2]. For a pure Xe discharge the simulations give a bulk electron temperature of 0.40 V and an electron density of 6.6×10^{15} m^{-3}. The plasma parameters derived from the simulations are listed in Table I. The presheath-sheath boundary x_o is determined by finding the location where the discharge starts to deviate from quasineutrality or where the charge density deviates from zero. The presheath-sheath boundary is located at 0.300 cm for pure argon discharge, 0.285 cm for pure xenon discharge and at 0.295 cm for Ar/Xe discharge, with an estimated uncertainty of 0.005 cm. The location of the presheath-sheath boundary is shown in Figs. 1 and 2. The effective electron temperature in the presheath region is shown in Fig. 3(a) and the ion temperature in the presheath region is shown in Fig. 3(b). The xenon ion temperature is roughly the same for a pure xenon discharge and Ar/Xe mixture, but becomes slightly higher as we approach the presheath-sheath boundary, in particular, for a pure xenon discharge.
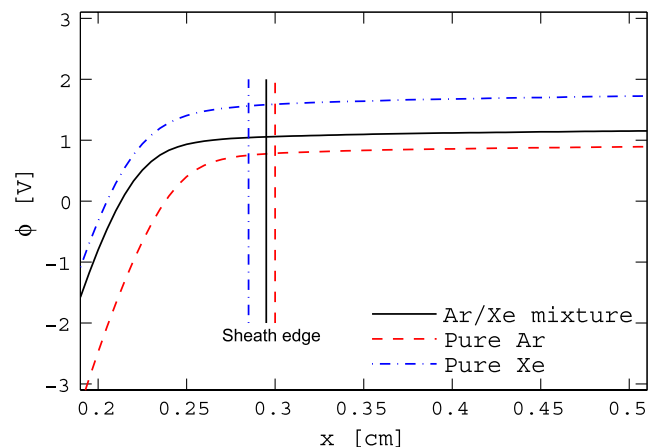

FIG. 1 (color online). The plasma potential versus distance from the biased plate for a pure argon discharge, an Ar/Xe discharge, and a pure xenon discharge at 0.7 m Torr.
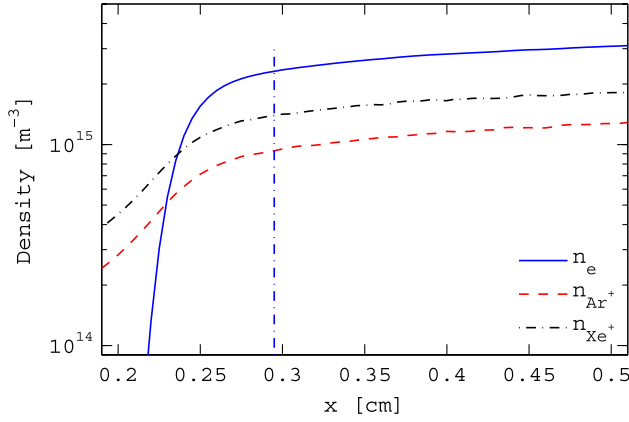
FIG. 2 (color online). The density profiles of the charged particles for an argon-xenon discharge with argon and xenon partial pressures 0.5 and 0.2 mTorr, respectively.

The argon ion temperature is higher for argon ions in an Ar/Xe mixture than for a pure argon discharge. Yip *et al.* [8] measured the ion temperature in the range 37–61 meV which is in a similar range as the simulation results.

 The velocities of argon and xenon ions versus the distance from the biased plate shifted by the location presheath-sheath boundary are shown in Fig. 4. For the Ar/Xe mixture the two ions have very distinct velocity profiles within the presheath; the argon ion has consistently higher velocity than the xenon ion. For a pure argon discharge the argon ion has almost the same velocity profile as it does in the mixture of argon and xenon. Similarly for a xenon discharge the xenon ion has almost the same velocity profile as it does in the mixture of argon and xenon. The velocity of the argon ion at the presheath-sheath boundary is 985 m/s for pure argon discharge and 926 m/s for the Ar/Xe mixture. The velocity of the xenon ion at the presheath-sheath boundary is 584 m/s for pure xenon discharge and 544 m/s for the Ar/Xe mixture. Thus the ion speed at the presheath-sheath boundary is roughly the same for an ion in a pure argon or xenon discharge and for the same ion in a mixture of argon and xenon. Using the bulk effective electron temperature for a pure argon discharge in Eq. (1) gives 898 m/s, and for a pure xenon discharge it gives 540 m/s. For Ar/Xe mixture it gives 907 m/s for argon ions and 501 m/s for xenon ions. Therefore we draw the conclusion from our simulation that each ion reaches its own Bohm speed at the presheath-sheath interface. These findings contradict the experimental findings of Lee *et al.* [1,2] where the ion velocities near the presheath-sheath
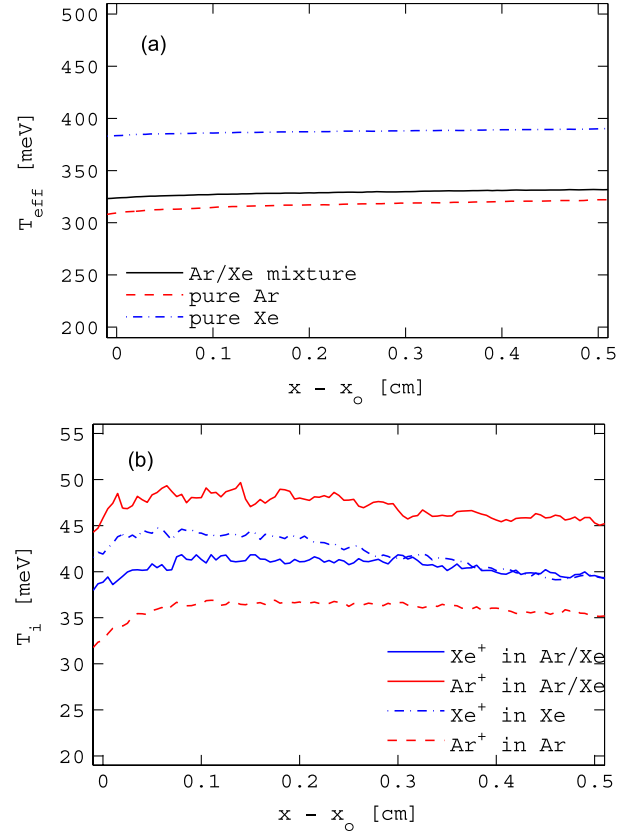

FIG. 3 (color online). The (a) effective electron temperature and (b) the ion temperature in the presheath region for a pure argon discharge, an Ar/Xe discharge and a pure xenon discharge at 0.7 m Torr.

boundary approach the common ion sound speed for both argon and xenon ions in the Ar/Xe discharge.

 For the Ar/He system [11] ion-ion two stream instabilities have been measured in the presheath, and they are strongest when the relative concentration of each ion species is similar [31]. Furthermore, Baalrud *et al.* [7] argue that ion-ion two stream instability leads to a collisional friction that slows down one ion species and accelerates the other, while this collisional friction can be ignored in a stable plasma. Thus to understand the simulation results, we have calculated the instability condition from kinetic theory. Including collisions and assuming drifting Maxwellian distributions for each species (electrons, Ar^+, and Xe^+), the wave dispersion is given by [32,33]

$$2k^2\lambda_e^2 = Z'(\zeta_e) + \sum_j (V_j/v_j)^2 Z'(\zeta_j), \qquad (3)$$

where k is the wavenumber, λ_e is the electron Debye length, $V_j = u_{B,j}(n_j/n_e)^{1/2}$ ($j = 1, 2$ corresponds to argon and xenon ions, respectively) are the density-weighted ion Bohm speeds, $v_j = (eT_j/M_j)^{1/2}$ are the ion thermal velocities, and Z' is the derivative of the plasma dispersion function $Z(\zeta) = i\pi^{1/2}e^{-\zeta^2}\text{erfc}(-i\zeta)$. The arguments of

TABLE I. The plasma parameters derived from the simulation

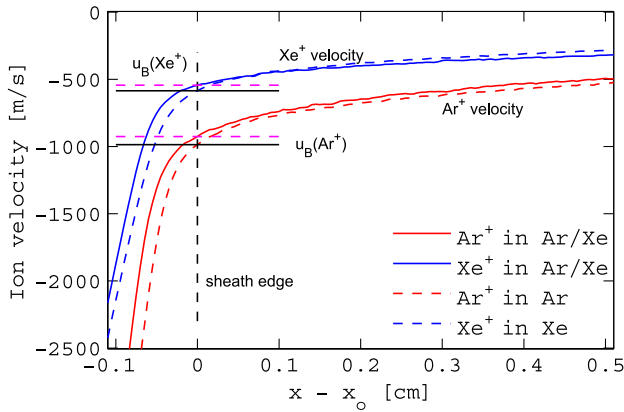| Disch.	T_{eff} [meV]	x_0 [cm]	$u_{B,Ar^+}^{T_{\text{eff}}}$ [m/s]	$u_{B,Xe^+}^{T_{\text{eff}}}$ [m/s]	$u_{B,Ar^+}^{x_0}$ [m/s]	$u_{B,Xe^+}^{x_0}$ [m/s]	$n_e/10^{15}$ [m^{-3}]
Ar	336	0.300	898	$\cdots$	985	$\cdots$	4.7
Ar/Xe	344	0.295	907	501	926	544	5.6
Xe	398	0.285	$\cdots$	540	$\cdots$	584	6.6

FIG. 4 (color online). The velocity of argon and xenon ions versus distance from the biased plate shifted by the location presheath-sheath boundary for a pure argon discharge, an Ar/Xe discharge and a pure xenon discharge at 0.7 m Torr. The solid horizontal lines show the Bohm speed determined at the presheath-sheath boundary for a pure argon and pure xenon discharge, respectively, and the dashed horizontal lines show the Bohm speed determined at the presheath-sheath boundary in an Ar/Xe mixture for argon and xenon ions, respectively.

Z' are $\zeta = (\omega/k + i\nu/k - u)/(2^{1/2}\nu)$, where ω is the radian frequency, u and ν are the drift and thermal velocities of the species, respectively, and ν is the collision frequency with the background gas. The least stable solutions of (3) are a slow (ion thermal) wave with phase velocity $\nu_{ph} \sim \nu_j$, and a fast (ion acoustic) wave with $\nu_{ph} \sim u_B$. Both fast and slow waves can be driven unstable if the relative ion drift velocity is large compared to the ion thermal velocities. Since the ion temperatures in the simulation are relatively uniform over the discharge length, the most unstable position is at the presheath-sheath edge. We have determined the stability of the wave solutions of (3) over the range of k's of interest. We find that for the simulation parameters, there is no instability. Reducing the ion temperatures 60% below the self-consistent simulation values, we obtain the onset of instability for the ion acoustic wave at $k\lambda_e \approx 0.44$. This corresponds to unrealistic (below room temperature) values of 19 meV for argon and 16 meV for xenon. Alternatively, increasing T_{eff} by a factor of 2.5 above the simulation value can lead to the onset of instability. In summary, we find in the simulation that the ions enter the sheath with their individual Bohm speeds, and we find no evidence of unstable waves in our simulation, which is the proposed mechanism [7] for a common system speed.

[1] D. Lee, G. Severn, L. Oksuz, and N. Hershkowitz, J. Phys. D **39**, 5230 (2006).
[2] D. Lee, N. Hershkowitz, and G. D. Severn, Appl. Phys. Lett. **91**, 041505 (2007).
[3] R. N. Franklin, J. Phys. D **33**, 3186 (2000).
[4] R. N. Franklin, J. Phys. D **36**, 34 (2003).
[5] D. Lee, L. Oksuz, and N. Hershkowitz, Phys. Rev. Lett. **99**, 155004 (2007).
[6] S. D. Baalrud, C. C. Hegna, and J. D. Callen, Phys. Rev. Lett. **103**, 205002 (2009).
[7] S. D. Baalrud and C. C. Hegna, Phys. Plasmas **18**, 023505 (2011).
[8] C.-S. Yip, N. Hershkowitz, and G. Severn, Phys. Rev. Lett. **104**, 225003 (2010).
[9] D. Bohm, in *The Characteristics of Electrical Discharges in Magnetic Fields*, edited by A. Guthrie and R. K. Wakerling (McGraw-Hill, New York, 1949), Chap. 3, pp. 77–86.
[10] K.-U. Riemann, IEEE Trans. Plasma Sci. **23**, 709 (1995).
[11] G. D. Severn, X. Wang, E. Ko, and N. Hershkowitz, Phys. Rev. Lett. **90**, 145001 (2003).
[12] C. Birdsall, IEEE Trans. Plasma Sci. **19**, 65 (1991).
[13] J. Hammel and J. P. Verboncoeur, Bull. Am. Phys. Soc. **48**, 66 (2003).
[14] J. P. Verboncoeur, A. B. Langdon, and N. T. Gladd, Comput. Phys. Commun. **87**, 199 (1995).
[15] V. Vahedi and M. Surendra, Comput. Phys. Commun. **87**, 179 (1995).
[16] J. Ferch, B. Granitza, C. Masche, and W. Raith, J. Phys. B **18**, 967 (1985).
[17] F. J. de Heer, R. H. J. Jansen, and W. van der Kaay, J. Phys. B **12**, 979 (1979).
[18] M. Hayashi, Cross sections, http://jila.colorado.edu/~avp/collision_data/electronneutral/hayashi.txt
[19] E. Eggarter, J. Chem. Phys. **62**, 833 (1975).
[20] E. Krishnakumar and S. K. Srivastava, J. Phys. B **21**, 1055 (1988).
[21] D. Vikor, M. Minic, I. Cadez, and M. Kurepa, Fizika (Zegreb) **21**, 345 (1989).
[22] W. H. Cramer, J. Chem. Phys. **30**, 641 (1959).
[23] A. V. Phelps, C. H. Greene, and J. P. Burke, J. Phys. B **33**, 2965 (2000).
[24] R. Hegerberg, M. T. Elford, and H. R. Skullerud, J. Phys. B **15**, 797 (1982).
[25] A. Mozumder, J. Chem. Phys. **72**, 6289 (1980).
[26] S. Nakazaki, K. A. Berrington, W. B. Eissner, and Y. Itikawa, J. Phys. B **30**, 5805 (1997).
[27] Y. Sakai, S. Sawada, and H. Tagashira, J. Phys. D **24**, 283 (1991).
[28] D. Rapp and P. Englander-Golden, J. Chem. Phys. **43**, 1464 (1965).
[29] A. V. Phelps, Cross sections, http://jilacolorado.edu/~avp/collision_data/neutralneutral/atomatom.txt
[30] D. Piscitelli, A. V. Phelps, J. de Urquijo, E. Basurto and L. C. Pitchford, Phys. Rev. E **68**, 046408 (2003).
[31] N. Hershkowitz, Phys. Plasmas **12**, 055502 (2005).
[32] M. Tuszewski and S. P. Gary, Phys. Plasmas **10**, 539 (2003).
[33] E. Kawamura, A. J. Lichtenberg, and M. A. Lieberman, J. Appl. Phys. **107**, 123301 (2010).